Switching the curl of polarization vectors by an irrotational electric field

Fei Xue, Linze Li, Jason Britson, Zijian Hong, Colin Andrew Heikes, Carolina Adamo, Darrell G. Schlom, Xiaoqing Pan, and Long-Qing Chen

Phys. Rev. B **94**, 100103 — Published 26 September 2016

DOI: 10.1103/PhysRevB.94.100103

Switching the curl of polarization vectors by an irrotational electric field

Fei Xue,[1] Linze Li,[2] Jason Britson,[1] Zijian Hong,[1] Colin Andrew Heikes,[3] Carolina Adamo,[3] Darrell G. Schlom,[3,4] Xiaoqing Pan,[2] and Long-Qing Chen[1]

[1]Department of Materials Science and Engineering, The Pennsylvania State University, University Park, Pennsylvania 16802, USA

[2]Department of Materials Science and Engineering, University of Michigan, Ann Arbor, Michigan 48109, USA

[3]Department of Materials Science and Engineering, Cornell University, Ithaca, New York 14853, United States

[4]Kavli Institute at Cornell for Nanoscale Science, Ithaca, New York 14853, USA

Ferroelectric vortex domains are of significant interest due to their rich physics and potential applications. Here, we propose the crystallographic, strain, and electric conditions for spontaneous vortex domains and study the influence of oxygen octahedral tilt on vortex wall orientations. Using 109° domain walls in $BiFeO_3$ films as an example, it is demonstrated that vortex domains result from bound charge density waves, i.e., from alternating positive and negative bound charges. The vortex domains lead to a net curl of the polarization vectors that can be switched by an irrotational electric field.

PACS number: 41.20.Cv, 61.46.-w, 77.55.Nv, 77.80.Dj

In ferroic materials, polarization and magnetization vectors may rotate around a point and form flux-closure domains, i.e., vortex domains. Although magnetic vortex domains are well known [1], polar vortex domains have only recently been observed and investigated [2-6]. Polar vortex domains are typically caused by either reduced size in three dimensions, such as in ferroelectric nanodots or nanoislands, without charge compensation on the surfaces [7-9], or induced by local external electric fields, e.g., from a piezoresponse force microscope [10,11]. Although spontaneous vortex domains in ferroelectric thin films have been experimentally observed in $PbZr_xTi_{1-x}O_3$ and $BiFeO_3$ (BFO) [12-14], the necessary conditions for forming vortex domains in a heterostructure, e.g., a ferroelectric film on a substrate or one-dimensional superlattice (finite size in one dimension) are not known. Furthermore, the usefulness of these observed domains has been questionable due to the inability to reverse the chirality of the static vertices under experimental conditions.

BFO is a room-temperature antiferromagnet and ferroelectric, with spontaneous electric polarization along the pseudocubic body diagonal directions, as sketched in Fig. 1(a) [15]. The ferroelectric domains form 71°, 109°, and 180° walls, with the angles denoting the change of polarization directions across the domain walls. Vortex domains resulting from 180° polarization rotations within triangular-shaped domains have been observed near the intersection between vertical 109° domain walls and the film/substrate interface in $(001)_p$-orientated BFO films (where the subscript p indicates pseudocubic indices), as illustrated in Fig. 1(c) [13,16]. We will refer to this vortex domain configuration as 109/180 vortex domains.

Besides having ferroelectric and antiferromagnetic orders, BFO also shows an out-of-phase oxygen octahedral tilt pattern, which is described by an axial vector. As shown in Figs. 1(e) and 1(f), the direction of the axial vector is chosen to be along the rotation axis of one octahedron, and the two situations with the axial vector parallel and antiparallel to the polarization direction are energetically degenerate [17]. Furthermore, the corner-sharing network of oxygen octahedra serves as the "skeleton" of the crystal, and the distortion of the tilt vectors costs substantial energy [18]. Due to the possibility of the polarization and tilt vectors being antiparallel and the substantial energy cost related to the tilt vectors, the domain wall energy hierarchy in BFO becomes 109° < 180° < 71°, rather than the expected 71° < 109° < 180° [17-20].

In this Letter we propose the basic crystallographic, electric, and strain conditions for the formation of vortex domain structures in ferroelectric thin films and demonstrate that the handedness of these structures can be switched with experimentally accessible electric fields. The conditions are illustrated using the 109° domain walls in BFO as an example, based on the Ginzburg-Landau-Devonshire theory with the equilibrium equations solved by the phase-field method [21,22]. From the phase-field simulations, we not only reveal the underlying origins of the vortex domains, but also show the significant contribution of the oxygen octahedral tilt to the vortex domain stability ignored in prior theoretical analyses.

We show that two conditions are required for the spontaneous generation of vortex domains in ferroelectric films or superlattices. The first is an interface separating a ferroelectric film from a nonpolar insulator. This can be easily realized by well-developed film growth techniques [23]. The interface locally reduces the polarization

components perpendicular to the interface to minimize the depolarization field. The second is a driving force maintaining the overall polarization component perpendicular to the interface. The driving force can be a compressive strain due to the mismatch between the film and substrate, or a crystallographic constraint as in the case of the $(001)_p$ BFO films. Note that the first condition is short-range with an influence local to the interface, whereas the second condition is global to the whole system.

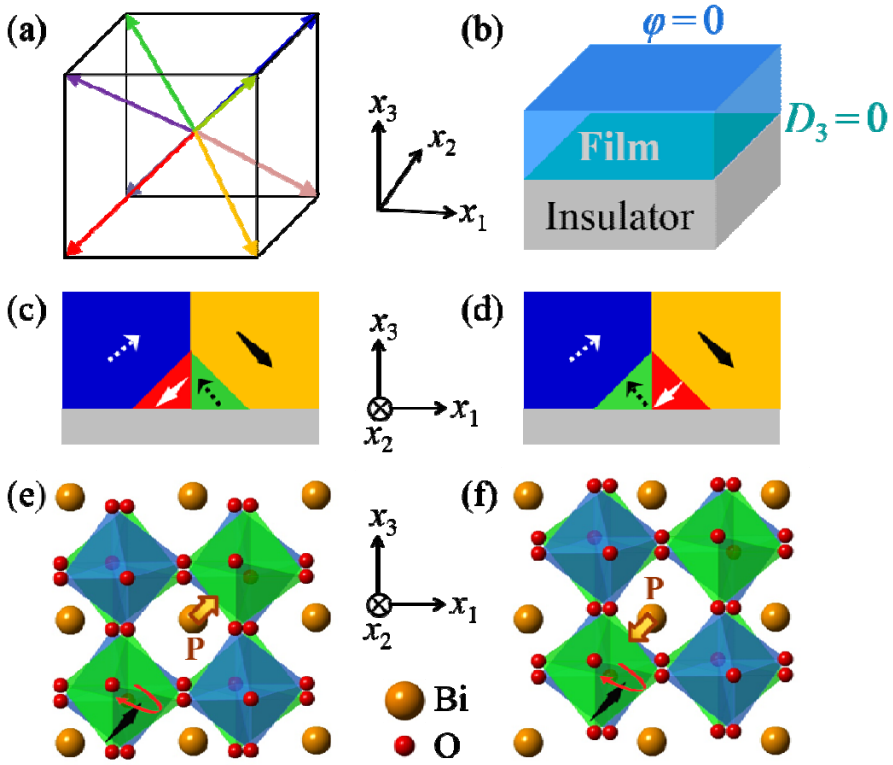

FIG. 1. (a) Symmetry allowed polarization directions in BFO. (b) A schematic of the electrical boundary conditions of the BFO films. (c) A schematic of the vortex domains with the combination of 109° and 180° walls (109/180 vortex domains). (d) A schematic of the vortex domains with the combination of 109° and 71° walls (109/71 vortex domains). (e) and (f) Crystal structures of BFO with the same rotation axis (tilt vectors) and antiparallel polarization vectors, as labeled by the black and orange arrows, respectively.

To demonstrate the formation of vortex domains under the above conditions, the 109° domain walls in the $(001)_p$ BFO films under a small epitaxial strain are studied as a model system. We choose the 109° domain walls since they have the lowest wall energy in BFO [18-20].

In the phase-field simulations, both polarization, $P_i (i = 1-3)$, and oxygen octahedral tilt order parameters, $\theta_i (i = 1-3)$, are incorporated [21,24,25]. The total free energy includes the contributions from the Landau bulk free energy, gradient energy, elastic energy, and electrostatic energy [18,26].

$$F = \int_V [\alpha_{ij} P_i P_j + \alpha_{ijkl} P_i P_j P_k P_l + \beta_{ij} \theta_i \theta_j + \beta_{ijkl} \theta_i \theta_j \theta_k \theta_l + t_{ijkl} P_i P_j \theta_k \theta_l + \frac{1}{2} g_{ijkl} \frac{\partial P_i}{\partial x_j} \frac{\partial P_k}{\partial x_l} + \frac{1}{2} \kappa_{ijkl} \frac{\partial \theta_i}{\partial x_j} \frac{\partial \theta_k}{\partial x_l} + \frac{1}{2} c_{ijkl} (\varepsilon_{ij} - \varepsilon_{ij}^0)(\varepsilon_{kl} - \varepsilon_{kl}^0) - E_i P_i - \frac{1}{2} \varepsilon_0 \kappa_b E_i E_i] dV \quad , \quad (1)$$

where $\alpha_{ij}, \alpha_{ijkl}, \beta_{ij}, \beta_{ijkl}$, and t_{ijkl} are coefficients of the Landau polynomial under stress-free boundary conditions, g_{ijkl} and κ_{ijkl} are the gradient energy coefficients, x_i is the spatial coordinate, c_{ijkl} is the elastic stiffness tensor, ε_{ij} and ε_{kl}^0 are the total strain and eigenstrain, respectively, E_i is the electric field, ε_0 is the permittivity of free space, and κ_b is the background dielectric constant [27].

Since the coupling term $t_{ijkl} P_i P_j \theta_k \theta_l$ is biquadratic, the parallel and antiparallel orientations of $[P_1 P_2 P_3]$ and $[\theta_1 \theta_2 \theta_3]$ are energetically degenerate, as shown in Figs. 1(e) and 1(f). The eigenstrain is related to the order parameters through $\varepsilon_{ij}^0 = \lambda_{ijkl} \theta_k \theta_l + h_{ijkl} P_k P_l$,

where λ_{ijkl} and h_{ijkl} are coupling coefficients [28]. The electric field is calculated by $E_i = -\frac{\partial \varphi}{\partial x_i}$ with φ denoting the electrostatic potential.

As shown in Fig. 1(b), the electrical boundary conditions of the top surface and bottom interface are set as short-circuit with $\varphi = 0$ and open-circuit with $D_3 = P_3 - \varepsilon_0 \kappa_b \frac{\partial \varphi}{\partial x_3} = 0$, respectively [25]. The boundary conditions simulate the situation that the bottom interface has uncompensated bound charges due to a nonpolar insulator substrate, whereas the top surface is compensated by unavoidable screening charges adsorbed from the air [13,29].

The mechanical and electrostatic equilibrium equations are solved using the methods described in Refs. [24,25]. All of the coefficients are listed in the supplementary materials of Ref. [18]. The phase-field equations are solved with periodic boundary conditions along the in-plane x_1 and x_2 directions, and a superposition method is used along the x_3 direction [22,24]. The system size is $128\Delta x \times 128\Delta x \times 20\Delta x$, with a grid spacing $\Delta x = 0.38 nm$.

First, the 109° domain walls in Fig. 2(a) are analyzed to determine the driving force for the formation of vortex domains. The 109° walls separate two domains, which are denoted by $[111,111]$ and $[1\bar{1}\bar{1},\bar{1}11]$ with the notation $[P_1P_2P_3,\theta_1\theta_2\theta_3]$ labeling the order parameters in a domain [18]. The two domains are modulated along the $[100]_p$ direction, and the depolarization field is reduced by the alternating upward and downward polarization components [30,31]. Due to the presence of the electrically

insulating substrate, the depolarization field tends to reduce the polarization component P_3 near the bottom interface, and the polarization gradient gives rise to a bound charge density expressed by $\rho_b = -\frac{\partial P_3}{\partial x_3}$.

The upward and downward polarization components result in alternating positive and negative bound charges, as plotted in Fig. 2(b). The modulation of the bound charges further induces an in-plane electric field alternating between $+x_1$ and $-x_1$, as shown in Fig. 2(c). The electric field pointing to $+x_1$ lies along the same direction as the original P_1, which increases the magnitude of P_1. The electric field along $-x_1$, however, acts against the original P_1. Consequently, small triangular-shaped domains with switched P_1 are nucleated at one half of the domain walls, as shown in Fig. 2(d). The polarization vectors show continuous rotations and form flux-closure vortex domains, as shown in Fig. 2(e). The vortex domains consist of two 109° walls and two 71° walls, which we call the 109/71 vortex domains as illustrated in Fig. 1(d). These are different from the previously discussed 109/180 vortex domains [13].

Similar vortex domains are observed in BFO films by atomic-scale high-angle annular-dark-field (HAADF) scanning transmission electron microscopy (STEM) imaging, as shown in Figs. 2(f) and S6. Following the previous work [13,32], the HAADF STEM image was processed to generate a unit-cell-by-unit-cell map of the polarization vectors. In both Figs. 2(e) and 2(f), P_3 is reduced near the bottom interface. While the experimentally observed continuous rotation of the polarization vectors generally follows the calculated domain patterns shown in Fig. 2(e), there are subtle

differences in the polarization directions and magnitudes near the vortex cores. It should be pointed out that the polarization vector distribution in the experiment is subject to measurement errors and can be affected by the presence of unavoidable defects in the sample such as oxygen vacancies. Therefore, the agreement between the simulation and experimental mappings is only considered to be qualitative.

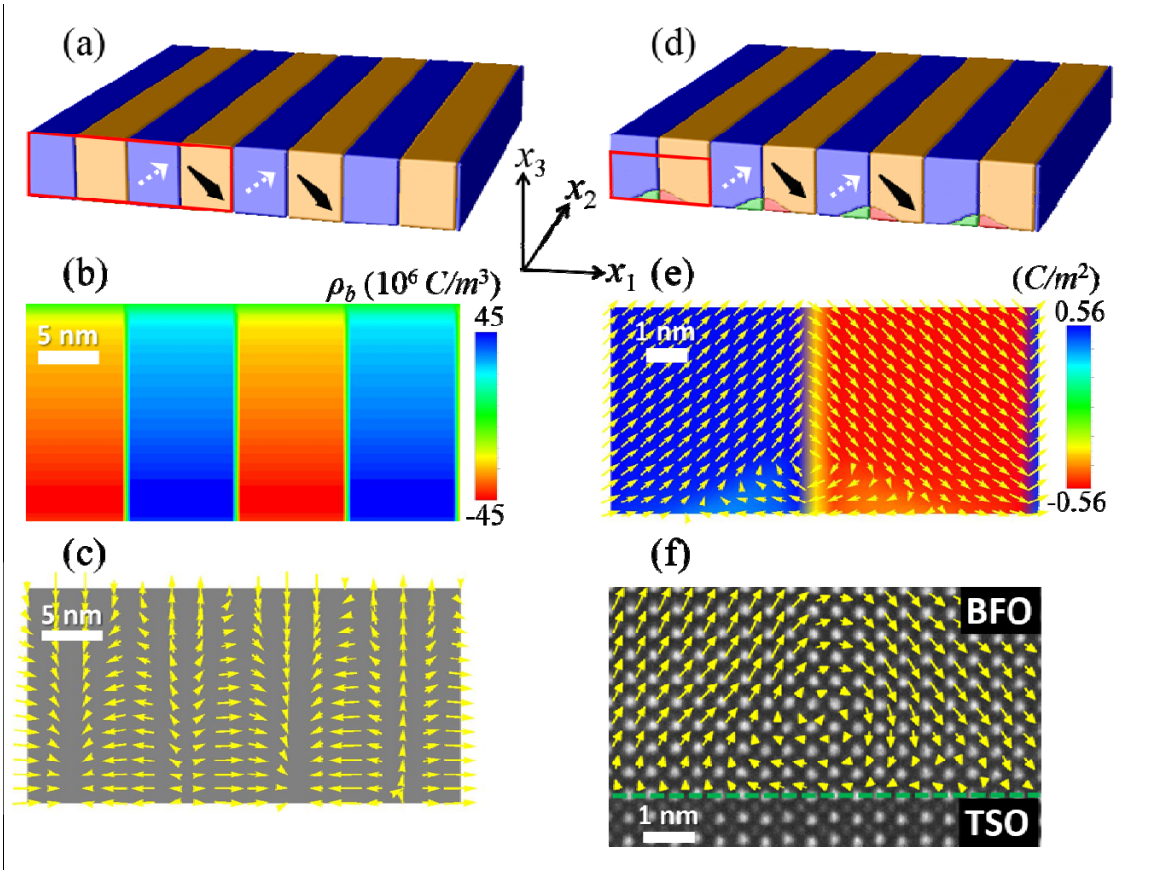

FIG. 2. The origin of vortex domains in BFO films. (a) 109° domain walls without vortex domains. (b) The distribution of bound charges within the rectangular region in (a). (c) The distribution of electric fields induced by the bound charges in (b). (d) 109/71 vortex domains from a phase-field simulation. (e) Polarization vectors within the region noted by the rectangle in (d). The color in (e) represents the polarization component out of the plane of the page. (f) Experimental HAADF STEM image of a 5 nm think BFO film grown on a (110) $TbScO_3$ substrate. The overlaid yellow vectors show the polarization distributions calculated from the atomic displacements between the Fe and Bi atoms. (a), (b), and (c) represent unstable structures, and are plotted to explain the origin of the vortex domains in (d) and (e).

The vortex domains in a ferroelectric film or superlattice are caused by the competition between the Landau bulk free energy (or elastic energy) and electrostatic energy. Under large compressive strains or due to crystallographic constraint, e.g., rhombohedral phases in $(001)_p$ films, the out-of-plane polarization component is unavoidable. Subjected to open-circuit boundary conditions, on either one or two interfaces, the ferroelectric domains tend to exist with alternating upward and downward polarization components to reduce the overall depolarization fields, leading to alternating positive and negative bound charges near the uncompensated interface. The bound charges yield an internal in-plane electric field, which gives rise to vortex domains near the domain walls. Here, in the main text, we show that vortex domains can be caused by the competition between the Landau bulk free energy and electrostatic energy, while the supplementary materials we show an example of vortex domains resulting from a large compressive strain in a tetragonal system.

If only one interface is in contact with an insulating nonpolar substrate as shown in Fig. 1(b), vortex domains are induced near the uncompensated interface. When both interfaces to the ferroelectric are subjected to insulating materials, as in the case of superlattices or multilayers [14], vortex domains are formed near both interfaces, and the vortex domains near the 109° domain walls in BFO films with open-circuit boundary conditions on both interfaces are demonstrated in the supplementary materials.

When set as initial configurations in the phase-field simulations, the 109/180 vortex domains are found to be stable. Within the triangular-shaped regions, the polarization vectors in Fig. 3(c) are rotated by 180°, whereas the oxygen octahedral tilt vectors in Fig. 3(e) exhibit almost no change since the polarization can be parallel or

antiparallel to the tilt vectors. On the other hand, in the 109/71 vortex domains, although the polarization is rotated by 71° in the triangular-shaped regions, the tilt vectors do not change significantly due to the substantial energy cost related to the variation of the tilt vectors, as shown in Fig. 3(f). With the polarization and tilt vectors not parallel or antiparallel, the magnitude of the polarization vectors in the triangular-shaped regions is reduced, as shown in Figs. 2(e) and 2(f).

The stabilities of the two types of vortex domains are determined by the competition between the differences of bulk energy and interfacial energy, i.e., dependent on the length scale. Since the angles between the polarization and tilt vectors in the triangular-shaped regions of the 109/71 vortex domains are quite different from the equilibrium values, leading to larger bulk energy, the 109/180 vortex domains is more energetically favorable when the triangular-shaped regions are sufficiently large, and experimentally the 109/180 vortex domains is observed in BFO films thicker than 20 nm [13]. When the film thickness becomes 5 nm, with the domain width reduced and the triangular-shaped regions shrinking correspondingly, the interfacial energy dominants, and the 109/71 vortex domains, with smaller polarization variation, are more energetically favorable. Therefore, both types of vortex domains are stabilized in the phase-field simulations and observed experimentally in BFO films; the appearance of each structure depends on film thickness.

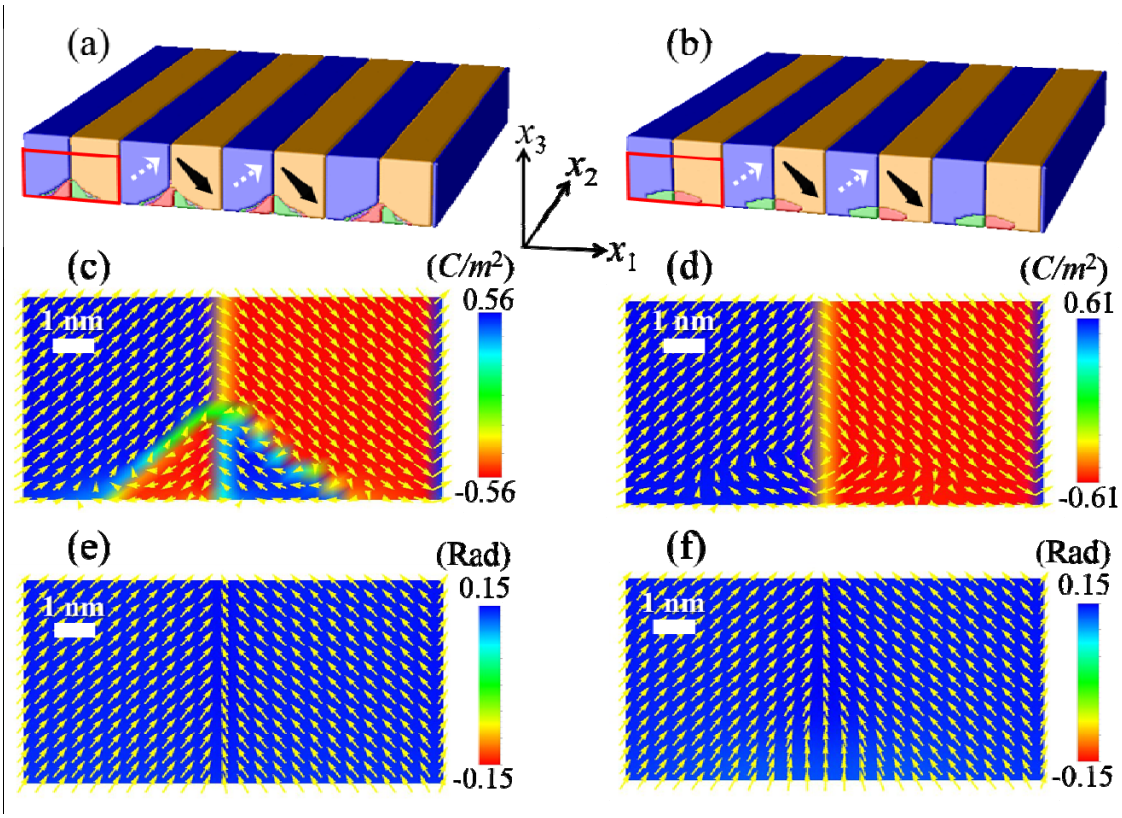

FIG. 3. Vortex domains in rhombohedral systems with and without oxygen octahedral tilt. (a) and (b) Domain structures in 109° domain walls with and without oxygen octahedral tilt, respectively. (c) and (d) Polarization vector distributions within the regions denoted by the rectangles in (a) and (b), respectively. (e) and (f) Distribution of the tilt vectors in the 109/180 and 109/71 vortex domains, respectively. The color in (c), (d), (e), and (f) represents the vector component out of the plane of the page. The color bars for the tilt vectors in (e) and (f) are in full scale, to emphasize the small variation of the out-of-plane tilt component.

Based on phase-field simulations, we also investigated the effect of the oxygen octahedral tilt on the formation of the vortex domains. The tilt order parameter is maintained at zero in the simulations, i.e., $\theta_i = 0 (i = 1-3)$, which is the case for the rhombohedral phase in the classic ferroelectrics, e.g., rhombohedral $BaTiO_3$. Again the 109° domain walls are analyzed for comparison (for vortex domains near 71° and 180° walls, see supplementary materials). In the 109° domain walls, separating the domains $[111,000]$ and $[1\bar{1}\bar{1},000]$, the vortex domains in Figs. 3(b) and 3(d) are similar to 109/71 vortex domains with oxygen octahedral tilt, as shown in Fig. 2(e). With

polarization as the only order parameter, however, the 109/180 vortex domains are unstable when set as the initial conditions in the simulations, and the 180° walls change to 71° walls (the instability of the 109/180 vortex domains is independent of film thickness). This is because the domain wall energy of 180° walls is much larger than that of the 71° walls with polarization as the only order parameter [33], and the electric field induced by the bound charges only has in-plane components, as shown in Fig. 2(c). Therefore, the oxygen octahedral tilt plays a significant role in stabilizing the 109/180 vortex domains.

Next the switching process of the vortex domains under external electric fields will be demonstrated. One unique property of rhombohedral domains is the net curl of the polarization vectors. As shown in Fig. 2(c), the induced electric field is symmetric along the x_1 direction. The resulting vortex domains are, however, asymmetric, and only appear on one side of the original domains, since the original domain structures are asymmetric with a positive P_1, which suppresses one half of the possible vortex domains as shown in Figs. 2(e), 3(c), and 3(d). If we name clockwise vortex domains as vortices, and counterclockwise vortex domains as anti-vortices, Figs. 2(e), 3(c), and 3(d) only show vortices; anti-vortices are suppressed, which results in a net curl. This is different from the situations of thin films and superlattices in a tetragonal structure, where the vortices and anti-vortices are paired, and the net curl is zero [12,14].

As discussed above, it is determined by the sign of P_1 whether the vortices or anti-vortices survive, and thus the vortices can be switched to anti-vortices if P_1 can be flipped by adding an in-plane electric field. In the phase-field simulations, an in-plane

electric field with increment $\Delta E_1 = 6.0\times10^6 V/m$ is applied to the system, and 2,000 simulation steps are given for the relaxation at a specific electric field (for the details about how to apply in-plane electric fields, see supplementary materials and Ref. [34]). The domain structures in Fig. 2(c) are set as the initial domain structures with the nonzero curl component $C_2 = (\nabla \times \vec{P})_2$.

The phase-field simulation results for the switching process are given in Fig. 4. As shown in Fig. 4(a), the change of P_1 produces a classical P-E hysteresis loop, and the net curl C_2 also forms a hysteresis loop. At point *B*, the vortices give rise to a positive C_2, as shown in Fig. 4(b). When the electric field changes from the point *B* to point *C*, P_1 decreases, whereas C_2 increases. This is because the net curl comes from the polarization vectors in the triangular-shaped regions with the local P_1 opposite to the overall P_1. Compared with Fig. 4(b), Fig. 4(c) shows larger triangular-shaped regions, and consequently smaller P_1 and larger C_2. For the same reason, C_2 reaches its maximum before switching. In addition, when the electric field increases from negative to zero, i.e., at the point *D*, the polarization vectors only show anti-vortices, as demonstrated in Fig. 4(d). Therefore, when P_1 flips its sign under the applied electric field, the vortex domains can be switched between vortices and anti-vortices with the locations shifted, which results in the switching of C_2. Note that the vortex domains in Figs. 4(b) and 4(d) are both stable after the removal of the external electric fields, and can potentially serve as the units of information memory storage.

Intuitively, the vortex domains should be switched by a vortex electric field [35,36]. It may be challenging, however, to generate a large vortex electric field at the nanoscale. Here, based on the fact that the survived vortex domains are determined by the overall in-plane polarization component, it is proposed that the curl can be switched by applying an irrotational in-plane electric field. Note that the coercive fields in the phase-field simulations are larger than that of the experimental measured value (75 kV/cm using planar electrodes on constrained BFO films [34]). This is reasonable since defects and thermal fluctuations are neglected in the model.

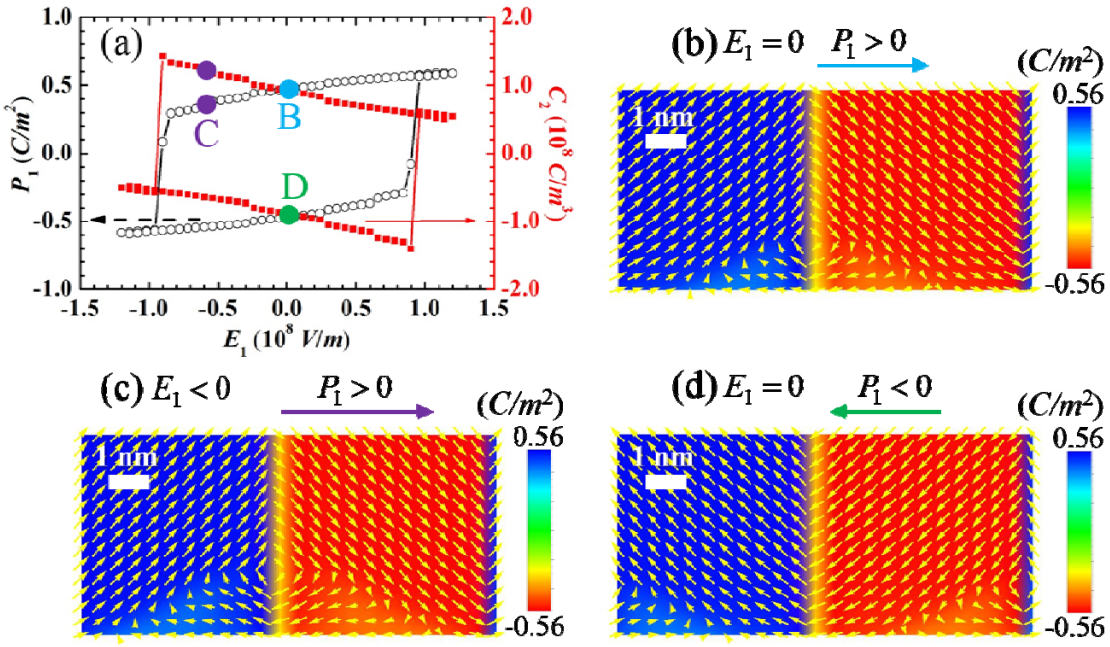

FIG. 4. Switching the curl of the polarization vectors. (a) Hysteresis loops of the polarization and curl components. (b)-(d) Polarization vector distributions corresponding to the points *B*, *C*, and *D* in (a), respectively. The plotted region corresponds to the red rectangular in Fig. 2(d), and the color in (b), (c), and (d) represents the polarization component out of the plane of the page. The arrows on top of (b), (c), and (d) indicate the overall magnitude of P_1.

In summary, we propose conditions to produce vortex domains in ferroelectric films and superlattices. Using $BiFeO_3$ film as an example, the underlying mechanism of the vortex domains is revealed, and two types of vortex domains are predicted for 109° domain walls, both of which are experimentally observed. Oxygen octahedral tilt may alter the relative stability of vortex domains. Also, it is shown that the net curl of the polarization vectors can be switched by applying a homogenous in-plane electric field. With well-developed film growth techniques, the proposed conditions may open a new route for engineering vortex domain structures in ferroelectric thin films and superlattices.

Acknowledgement:

The work at Penn State was supported by the U.S. Department of Energy (DOE), Office of Basic Energy Sciences, Division of Materials Sciences and Engineering under Award FG02-07ER46417 (FX, JB & LQC) and partially by the NSF MRSEC under Grant No. DMR-1420620 (FX) and No. DMR-1210588 (ZJH). The work at University of Michigan was supported by DOE under grant DE-FG02-07ER46416. The work at Cornell University was supported by the NSF (Nanosystems Engineering Research Center for Translational Applications of Nanoscale Multiferroic Systems) under grant number EEC-1160504. The authors would also like to acknowledge the National Center for Electron Microscopy at Lawrence Berkeley National Laboratory for their support under the DOE grant DE-AC02-05CH11231 for user facilities.

References

[1] C. Kittel, Reviews of Modern Physics **21**, 541 (1949).
[2] I. I. Naumov, L. Bellaiche, and H. Fu, Nature **432**, 737 (2004).
[3] I. I. Naumov and A. M. Bratkovsky, Physical review letters **101**, 107601 (2008).
[4] J. Wang, M. Kamlah, T.-Y. Zhang, Y. Li, and L.-Q. Chen, Applied physics letters **92**, 162905 (2008).
[5] R. G. P. McQuaid, L. J. McGilly, P. Sharma, A. Gruverman, and J. M. Gregg, Nature communications **2**, 404 (2011).
[6] L. Van Lich, T. Shimada, K. Nagano, Y. Hongjun, J. Wang, K. Huang, and T. Kitamura, Acta materialia **88**, 147 (2015).
[7] B. J. Rodriguez, X. S. Gao, L. F. Liu, W. Lee, I. I. Naumov, A. M. Bratkovsky, D. Hesse, and M. Alexe, Nano letters **9**, 1127 (2009).
[8] L. J. McGilly and J. M. Gregg, Nano letters **11**, 4490 (2011).
[9] L.-W. Chang, V. Nagarajan, J. F. Scott, and J. M. Gregg, Nano letters **13**, 2553 (2013).
[10] Y. Ivry, D. P. Chu, J. F. Scott, and C. Durkan, Physical review letters **104**, 207602 (2010).
[11] N. Balke *et al.*, Nature physics **8**, 81 (2012).
[12] C.-L. Jia, K. W. Urban, M. Alexe, D. Hesse, and I. Vrejoiu, Science **331**, 1420 (2011).
[13] C. T. Nelson *et al.*, Nano letters **11**, 828 (2011).
[14] Y. L. Tang *et al.*, Science **348**, 547 (2015).
[15] G. Catalan and J. F. Scott, Advanced Materials **21**, 2463 (2009).
[16] Y. Qi, Z. Chen, C. Huang, L. Wang, X. Han, J. Wang, P. Yang, T. Sritharan, and L. Chen, Journal of Applied Physics **111**, 104117 (2012).
[17] O. Diéguez, P. Aguado-Puente, J. Junquera, and J. Íñiguez, Physical Review B **87**, 024102 (2013).
[18] F. Xue, Y. Gu, L. Liang, Y. Wang, and L.-Q. Chen, Physical Review B **90**, 220101 (2014).
[19] Y. Wang, C. Nelson, A. Melville, B. Winchester, S. Shang, Z.-K. Liu, D. G. Schlom, X. Pan, and L.-Q. Chen, Physical review letters **110**, 267601 (2013).
[20] A. Lubk, S. Gemming, and N. A. Spaldin, Physical Review B **80**, 104110 (2009).
[21] L.-Q. Chen, Annual review of materials research **32**, 113 (2002).
[22] L.-Q. Chen and J. Shen, Computer Physics Communications **108**, 147 (1998).
[23] D. G. Schlom, L. Q. Chen, X. Pan, A. Schmehl, and M. A. Zurbuchen, Journal of the American Ceramic Society **91**, 2429 (2008).
[24] Y. L. Li, S. Y. Hu, Z. K. Liu, and L.-Q. Chen, Acta materialia **50**, 395 (2002).
[25] Y. L. Li, S. Y. Hu, Z. K. Liu, and L.-Q. Chen, Applied physics letters **81**, 427 (2002).
[26] J. J. Wang, X. Q. Ma, Q. Li, J. Britson, and L.-Q. Chen, Acta materialia **61**, 7591 (2013).
[27] A. K. Tagantsev, Ferroelectrics **69**, 321 (1986).
[28] A. F. Devonshire, Advances in physics **3**, 85 (1954).
[29] D. D. Fong *et al.*, Physical review letters **96**, 127601 (2006).
[30] P. Marton, I. Rychetsky, and J. Hlinka, Physical Review B **81**, 144125 (2010).
[31] Y.-H. Chu, Q. He, C.-H. Yang, P. Yu, L. W. Martin, P. Shafer, and R. Ramesh, Nano letters **9**, 1726 (2009).
[32] L. Li *et al.*, Nano letters **13**, 5218 (2013).
[33] M. Taherinejad, D. Vanderbilt, P. Marton, V. Stepkova, and J. Hlinka, Physical Review B **86**, 155138 (2012).
[34] Z. Chen *et al.*, Physical Review B **86**, 235125 (2012).
[35] J. Wang and M. Kamlah, Physical Review B **80**, 012101 (2009).
[36] I. I. Naumov and H. Fu, Physical review letters **101**, 197601 (2008).